論文 / 著書情報
Article / Book Information

Title	Analysis of current-voltage characteristics of Au/pentacene/fluorine polymer/indium zinc oxide diodes by electric-field-induced optical second-harmonic generation
Authors	Shohei Nishi, Dai Taguchi, Takaaki Manaka, Mitsumasa Iwamoto
Citation	Journal of Applied Physics, 117, , 245502
Pub. date	2015, 1
Note	This article may be downloaded for personal use only. Any other use requires prior permission of the author and AIP Publishing. The following article appeared in Journal of Applied Physics, 117, , 245502 and may be found at http://dx.doi.org/10.1063/1.4923058.
Note	This file is author (final) version.

Analysis of current-voltage characteristics of Au/pentacene/fluorine polymer/indium zinc oxide diode by electric-field-induced optical second-harmonic generation

Shohei Nishi, Dai Taguchi, Takaaki Manaka, and Mitsumasa Iwamoto*

Department of Physical Electronics, Tokyo Institute of Technology,

2-12-1 S3-33, O-okayama, Meguro-ku, Tokyo 152-8552, Japan

*Email iwamoto@pe.titech.ac.jp

Abstract

By using electric-field-induced optical second-harmonic generation (EFISHG) measurement coupled with the conventional current-voltage (*I*-*V*) measurement, we studied the carrier transport of organic double-layer diodes with a Au/pentacene/fluorine polymer (FP)/indium zinc oxide (IZO) structure. The rectifying *I*-*V* characteristics were converted into the *I*-*E* characteristics of the FP and pentacene layers. Results suggest a model in which Schottky-type electron injection from the IZO electrode to the FP layer governs the forward electrical conduction ($V > 0$), where the space charge electric field produced in the FP layer by accumulated holes at the pentacene/FP interface makes a significant contribution. On the other hand, Schottky-type injection by accumulated

interface electrons from the pentacene layer to the FP layer governs the backward electrical conduction ($V < 0$). The electroluminescence (EL) generated from the pentacene layer in the region $V > 0$ verifies the electron transport across the FP layer, and supports the above suggested model.

Keywords: organic device, electric-field-induced optical second-harmonic generation, Maxwell-Wagner effect, space charge field

1. INTRODUCTION

Recently, organic devices have attracted considerable attention in electronics, and many R & D studies on them have been conducted worldwide [1]. The development of organic light-emitting diodes (OLEDs), organic field-effect transistors (OFETs), organic solar cells (OSCs), and organic memory devices is of particular interest [2, 3]. Accordingly, preparation methods, characterization methods, and organic-based circuit techniques have been intensively investigated along with the discovery of new synthetic organic semiconductor materials. Conventionally, the current-voltage (*I*-*V*) and capacitance-voltage (*C*-*V*) measurements are performed to analyze the carrier transport in organic devices [4]. The resulting *I*-*V* and *C*-*V* characteristics are analyzed by using a RC equivalent circuit model [5], e.g., in a study on metal-insulator-semiconductor (MIS) capacitors incorporating a polyimide (PI) layer as the gate insulator and regioregular P3HT as the active semiconductor layer [6], and a model of energy diagram for organic devices that illustrates the molecular energy level of organic semiconductors and the Fermi energy level of electrodes [7], e.g., in a study on Al/LiF/poly(spirofluorene)/Ba/Al memory diodes [8]. However, clarification of the carrier injection and transport mechanism is not easy owing to the complex organic device structure, the hysteresis behaviors mainly caused by the dielectric nature of organic semiconductor materials, and

other factors. That is, the *I*-*V* and *C*-*V* characteristics are useful for studying organic devices, but the actual experimental results lead to a puzzling situation that the carrier injection and transport are discussed on the basis of semiconductor device physics using the energy band theory [5], even in the case of double layer devices.

Accordingly, it is very helpful to develop a novel method that can directly probe the electric potential and electric field distributions in organic devices [9], and to use the developed method in combination with the *I*-*V* and *C*-*V* measurements. We have been developing method of electric-field-induced optical second-harmonic generation (EFISHG) measurement that can selectively and directly probe the electric fields in organic layers and in organic devices [10-12]. This motivated us to study the electrical carrier transport mechanism of a variety of organic double-layer diodes, while taking into account their electric field distribution. In this study, we used organic double-layer diodes with Au/pentacene/fluorine polymer (FP)/ indium zinc oxide (IZO) structure, which show a rectifying behavior. The *I*-*V* characteristics of the diodes were converted into the current-electric field (*I*-*E*) characteristics of the pentacene and FP layers, using the results of EFISHG measurement coupled with the *I*-*V* measurement. The results showed that Schottky-type electron injection from the IZO electrode to the FP layer governs the forward current ($V > 0$), whereas electrons that accumulate at the

pentacene/FP interface are the main contributors to Schottky-type electron injection into the FP layer in the case of a backward current ($V < 0$). The electroluminescence (EL) generated from the pentacene in the region $V > 0$ supports our model that electron transport occurs across the FP layer. The resulting carrier transport mechanism is considerably different from that observed for organic double-layer diodes with structures of Au/pentacene/polyimide (PI)/IZO [13], Au/6,13-bis(triisopropylsilylethynyl)-pentacene/PI/indium tin oxide (ITO) [14], IZO/ N,N'-di-[(1-naphthyl)-N,N'-diphenyl]-(1,1'-biphenyl)-4,4'-diamine/tris(8-hydroxy-quinolinato)aluminum(III)/Al [15], and Au/pentacene/poly(vinylidene fluoride-trifluoroethylene) [16], which we investigated in our previous studies. EFISHG coupled with the *I-V* measurement is helpful for analyzing the carrier transport mechanism of organic double-layer diodes, and thus enables the study of the electrical transport properties of organic semiconductor layers. In this paper, we describe our findings on the electrical transport mechanism in organic double-layer diodes with Au/pentacene/FP/IZO structure, which is governed by a Schottky-type injection-limited process due to charges that accumulate at the interface.

2. EXPERIMENTAL

2.1. Sample preparation

Figure 1(a) shows the double-layer organic diodes (Au/pentacene/FP/IZO) used in this study. The diodes were prepared as follows. Glass substrates with a patterned IZO electrode were cleaned in UV/ozone treatment apparatus, onto which a 30 nm-thick fluorine layer (Asahi Glass Co., CTL-809M) was deposited using a spin coating technique. Subsequently, a pentacene layer (thickness: 100 nm) and an Au electrode (thickness: 100 nm) were successively deposited by vacuum evaporation, where the process pressure and evaporation rate were < 10^{-5} Torr and 1 Å/s, respectively. The working electrode area of the diodes was A=3.1 mm^2. The fabricated double-layer diodes were sealed in a glass bottle with silica gel, before they were used in the measurements.

2.2. *I-V* and EFISHG measurements

The *I-V* characteristics were measured using the electrical circuit illustrated in Fig. 1(a), where the applied dc voltage was increased at a step of 0.1 V with a period of 2 s. Figure 1(a) also illustrates the experimental setup for the EFISHG measurement, which is the same as that used in our previous studies [17-19]. The details of the measurement are as follows. A probing laser beam (repetition rate 10 Hz, duration 4 ns, average power

10 mW) is supplied from an optical parametric oscillator (OPO) pumped by the third-harmonic light of a *Q*-switched Nd:YAG laser (wavelength: 1064 nm). The OPO allows the wavelength of the probing laser to be selected in the region 800–1120 nm. The laser beam is *p*-polarized and obliquely impinges on the sample with an incident angle of 45°. Consequently, the incident laser beam possesses a nonzero electromagnetic field in the film thickness direction, which allows us to probe the dc electric field in the film thickness direction (see Eq. (1)). The reflected fundamental laser beam (wavelength: λ) is eliminated using optical filters, whereas the generated EFISHG light (wavelength: λ/2) is selectively detected through a monochromator and a photomultiplier tube (PMT).

EFISHG is a nonlinear optical process and the intensity of the EFISHG light $I_{2\omega}$ emitted from the pentacene layer is given as [10, 20]

$$I_{2\omega} \propto \left|\vec{P}_{2\omega}\right|^2 = a\left|\vec{E}_1\right|^2, \quad \vec{P}_{2\omega} = \varepsilon_0 \chi^{(3)} \vdots \vec{E}_1 \vec{E}_\omega \vec{E}_\omega, \tag{1}$$

where $\vec{P}_{2\omega}$ and $\vec{E}_1$ are the second-order nonlinear polarization and the electrostatic dc field in the pentacene layer, respectively. ε_0 is the dielectric constant of vacuum. $\vec{E}_\omega$ is the electric field of the incident laser beam with the angular frequency ω. $\chi^{(3)}$ is the third-order nonlinear susceptibility of the pentacene layer and resonantly enhances a laser when the laser wavelength is half of that required for the optical transition of pentacene molecules. The FP and pentacene layers are mostly isotropic, and we assume that the

$\chi^{(3)}_{zzzz}$ component is the dominant contributor, taking the *z*-axis as the film thickness direction [21]. Figure 2 shows EFISHG spectra of the pentacene and FP layers measured at various voltages, where single-layer Al/pentacene/IZO and Al/FP/IZO devices were used. The EFISHG is activated in pentacene molecules at an SH wavelength of 430 nm (laser wavelength: 860 nm), whereas the SH light generated from the FP layer is negligible. As a result, we were able to selectively probe the dc electric field E_1 in the pentacene layer of Au/pentacene/FP/IZO double-layer diodes by choosing an SH wavelength of 430 nm. Note that the laser beam and SH light pass through the FP and pentacene layers without a significant optical loss at the wavelengths used in the measurement [22, 23]. The dc electric field in the FP layer, E_2, is calculated as $E_2 = 1/d_2 \cdot (V - E_1 d_1)$ using the relationship $V = E_1 d_1 + E_2 d_2$ (d_2: FP layer thickness). Using the electric fields E_1 and E_2 in combination with the *I*-*V* data, we can plot the *I*-*E* characteristics of the pentacene and FP layers.

Figures 1(b) and 1(c) illustrate the timing charts for the incident laser pulses and voltage application. The dc electric field in the pentacene layer is given by the sum of the external field $\vec{E}_e$, space charge field $\vec{E}_s$, and background field $\vec{E}_b$, $\vec{E}_1 = \vec{E}_e + \vec{E}_s + \vec{E}_b$ [24], where $\vec{E}_e$, $\vec{E}_s$, and $\vec{E}_b$ are dc fields. Note that the background field $\vec{E}_b$ is induced in films by the work function difference between the IZO and Al electrodes, the interfacial

electrostatic field caused by electrification at the metal-film interface, and other factors [25]. Accordingly, we conducted time-resolved measurements to clarify the origin of the electric field in the EFISHG measurement. The results showed that the external field and space charge field are formed in a manner similar to our previous study [26]. That is, $\vec{E}_e$ is formed with a circuit response time of t_{RC} ~ 100 ns (Laplace field), while $\vec{E}_s$ is formed with a response time of t_{MW} ~ 1 μs >> t_{RC} (Poisson field) if carrier injection is followed by Maxwell-Wagner-type charge accumulation at the double-layer interface [19, 26]. E_b is the internal dc electric field. As a result, EFISHG light generated at t = 0, t ~ t_{RC}, and t = t_{MW} probe the dc electric field $\vec{E}_b$, the Laplace field $\vec{E}_e + \vec{E}_b$ $(= \vec{E'}_1)$, and the Poisson field $\vec{E}_e + \vec{E}_s + \vec{E}_b$ $(= \vec{E''}_1)$, respectively. The generated SH intensity is proportional to the square of the electric field across the pentacene layer, $I_{2\omega} = a\left|\vec{E}_1\right|^2$. At t ~ t_{RC}, this electric field is given as $\left|\vec{E}_1\right|$ $(= \left|\vec{E'}_1\right|)$ $= 1/d_1 \cdot C_2/(C_1 + C_2)V + E_b$ (C_1, C_2: capacitances of pentacene and FP layers, respectively). At t = 0.1 s >> t_{MW}, owing to the presence of interfacial charges Q_s, the EFISHG is given by $I_{2\omega} = a\left|\vec{E''}_1\right|^2$, where $\vec{E''}_1 = 1/d_1 \cdot C_2/(C_1 + C_2)V - 1/d_1 \cdot Q_s/(C_1 + C_2) + E_b$. In our EFISHG measurement, we used a pulsed square-wave voltage (duty time t_d=300 ns, $t_{RC} < t_d < t_{MW}$) to probe E'_1 (Fig. 1(b)) and a dc voltage to probe $E"_1$ (Fig. 1(c)).

3. RESULTS AND DISCUSSION

A rectifying behavior was observed in the *I*-*V* characteristics of the Au/pentacene/FP/IZO double-layer diode, as shown in Fig. 1(d), where the voltage *V* was applied to the Au electrode with reference to the IZO electrode. We consider that if the pentacene and FP layers show p-type and n-type semiconductor behaviors, respectively, a rectifying diode behavior will appear, as shown in Fig. 1(d). However, it is too early to discuss the *I*-*V* characteristics of the double-layer diode (Au/pentacene/FP/IZO) in this manner, because we do not know yet how the electric fields are actually formed in the pentacene and FP layers. Actually, the FP layer is generally a good electrical insulator. To clarify the carrier mechanism responsible for the rectifying behavior in detail, we must determine the electric field distribution and the carrier injection property of the diodes.

Figures 3(a) and 3(b) show the EFISHG intensity dependence on the applied voltage *V* and the electric field E_1 in the pentacene layer, respectively. In the EFISHG measurement, the Laplace electric field E_e+E_b was probed at $t=t_d$ ($> t_{RC}$), while the Poisson field $E_e+E_s+E_b$ was probed at $t > t_{MW}$ (see section 2.2). Here, the Laplace electric field means that the associated fields are unrelated to the space charge field produced by excess injected carriers, whereas the Poisson field is related to the space charge field. From the Laplace field at $t = t_d$, we can clearly see the square dependence of the EFISHG

intensity, $I_{2\omega} = a\left|\vec{E}_e\right|^2$ with $a = 2.1\times10^{-10}$, where $I_{2\omega}$ is the EFISHG intensity and E_e is the Laplace field. For the Poisson field at $t > t_{MW}$, the EFISHG intensity deviates from the square dependence. These results suggest the model illustrated in Figs. 3(c) and 3(d), in which the presence of accumulated interface charges in the diode under the Poisson field condition leads to the rectifying *I*-*V* characteristics. In the region $V > 0$, the EFISHG intensity is nearly constant (see Fig. 3(a)), indicating that the holes injected from the Au electrode serve as carriers in the pentacene layer, leading to hole accumulation at the pentacene/FP interface. In other words, the accumulated holes act as a source of the space charge field E_s, which can cancel out the Laplace field E_e in the pentacene layer, i.e., $E_e + E_s = 0$, whereas it gives rise to a nonzero electric field in the FP layer, as shown in Fig. 3(c). In the region $V < 0$, the EFISHG is proportional to the square of the voltage, though its intensity slightly decreases under the Poisson field condition. That is, a nonzero electric field is formed in the pentacene layer in the region $V < 0$, as shown in Fig. 3(d).

Figure 4 shows the *I*-*E* characteristics of the pentacene and FP layers. Here, the results of the EFISHG measurement (Fig. 3(b)) were used with the *I*-*V* data in Fig. 1(d) in the manner described in section 2.2. The current flowing across the pentacene layer increases steeply at approximately $E \cong 0$, while it is blocked in the region $E < 0$. The current flowing across the FP layer increases in the region $E >$ 2 MV/cm. These results

account for the rectifying *I-V* behavior of the diode (see the model in Figs. 3(c) and 3(d)). In the region $V > 0$, holes are smoothly injected from the Au electrode to the pentacene layer, and sufficiently accumulate at the pentacene/FP interface, i.e., $E_1 = 0$. The accumulated holes give rise to a space charge field in the FP layer. This space charge field in the FP layer assists electron injection from the IZO electrode to the FP layer, resulting in the forward current flowing across the diode. On the other hand, in the region $V < 0$, electrons are injected from the Au electrode to the pentacene layer and then accumulate at the pentacene/FP interface. This electron accumulation is insufficient and a nonzero electric field is formed in the pentacene layer. In other words, the space charge field formed by electrons that accumulate at the interface is small and does not assist hole injection from the IZO electrode to the FP layer. Consequently, backward current is suppressed. These results indicate that asymmetric hole (Q_1) and electron (Q_2) accumulation, $|Q_1| > |Q_2|$, is the origin of the rectifying behavior of the Au/pentacene/FP/IZO diode. It is instructive to further discuss the potential role of the electric field in the diode. In the forward region ($V > 0$), the electric field in the pentacene layer remains constant (see Fig. 3(b)), whereas electric field in the FP layer increases with the forward voltage. As a result, the carrier transport in the FP layer is the dominant contributor to the memory effect, hysteresis behavior, and other phenomena, as was

reported previously [8, 27]. On the other hand, in the backward region ($V > 0$), the electric field increases in both the pentacene and FP layers owing to insufficient electron accumulation. The nonzero electric field in the pentacene layer can cause the drift of mobile ions, which is related to the stress-biasing effect, memory effect, and other effects in metal-insulator-semiconductor (MIS) diodes [6, 28]. That is, in the reverse voltage region, not only the insulating layer but also the semiconducting layer can be the origin of instabilities in the device. This is completely different from the case of inorganic devices, where the electric field in the semiconductor layer is usually zero, i.e., the potential distribution is flat in the bulk region.

Figure 5 shows a Schottky plot (ln(I)-$\sqrt{E}$) of the FP layer. For the region $V > 0$, from the slope of the plot, we obtain the Schottky parameter $\beta_s = \sqrt{\frac{e^3}{4\pi\varepsilon_2\varepsilon_0}}$ = 1.1×10^{-3} kT [J/(V/m)$^{0.5}$] (k: Boltzmann constant, T: temperature), and the relative dielectric constant of the FP is estimated to be 2.1 (T=300 K). This value is in good agreement with the dielectric constant of FP estimated by capacitance measurement [29]. On the other hand, for the region $V < 0$, the Schottky parameter β_s is smaller and is calculated to be 5.8×10^{-4} kT [J/(V/m)$^{0.5}$]. It is instructive here to note that the Schottky parameter should be $\beta_s = \sqrt{\frac{\varepsilon_1-\varepsilon_2}{\varepsilon_1+\varepsilon_2}\frac{e^3}{4\pi\varepsilon_2\varepsilon_0}}$ ($\varepsilon_1 = 4.2$: relative dielectric constant of pentacene [30]) for electrons injected from the pentacene layer to the FP layer owing to the electrostatic

mirror image effect [31]. The experimental plots in Fig. 5 for $V < 0$ clearly support this model.

To further verify the carrier transport mechanism proposed above, we measured the EL spectra of the diode at V = +20 V (forward) and – 20 V (backward) using a high-sensitivity detector, as shown in Fig. 6, though the EL intensity was very low. The EL spectrum at + 20 V (forward) has a maximum at a wavelength of 720 nm, clearly reflecting electron-hole recombination at pentacene molecules. This result supports our model of carrier transport, which was derived on the basis of the results of EFISHG measurement: holes are injected from the Au electrode and accumulate at the pentacene/FP interface, while electrons are injected from the IZO electrode to the FP layer. Consequently, EL is generated from the pentacene layer owing to the recombination of injected electrons with the holes that accumulate at the interface. On the other hand, no EL was observed at – 20 V (backward). These results also support our model derived on the basis of the results of EFISHG measurement: electrons are injected from the Au electrode to the pentacene layer, and then cross the FP layer without meeting holes in the backward region (V < 0). Note that the FP and pentacene layers are transparent at wavelengths exceeding 720 nm, at which the EL is enhanced.

As we described above, EFISHG measurement coupled with the conventional *I*-*V*

measurement is very effective for studying the carrier transport of organic double-layer diodes, because the *I-V* characteristics are easily converted into the *I-E* characteristics of the two layers. The derived *I-E* characteristics are very useful for determining the carrier transport mechanism.

4. CONCLUSION

By using EFISHG measurements in combination with *I-V* measurements, we analyzed the rectifying *I-V* behavior of the Au/pentacene/FP/IZO double-layer diode. In the region $V > 0$, holes accumulated at the pentacene/FP interface and produced a space charge field in the FP layer. This electric field assisted Schottky-type electron injection at the FP/IZO interface and resulted in a forward current across the diode. In the region $V < 0$, the injection of electrons from the pentacene layer to the FP layer dominates the backward current. EFISHG measurement in combination with *I-V* measurement is very effective for analyzing the carrier transport of the organic semiconductor layer in organic devices.

Acknowledgements

Part of this work was financially supported by a Grant-in-Aid for Scientific

Research (S) (No. 22226007) and a Grant-in-Aid for Young Scientists (A) (No. 25709022) from the Japan Society for the Promotion of Science (JSPS). D. T. acknowledges financial support for this project from the Takano Science Foundation.

References

1. *Organic Electronics, Materials, Manufacturing and Applications*, edited by H. Klauk (Wiley, Weinheim, 2006).
2. M. Pagliaro, G. Palmisano, and R. Ciriminna, *Flexible Solar Cells* (Wiley, Weinheim, 2008).
3. T. Tsujimura, *OLED Display Fundamentals and Applications* (Wiley, Weinheim, 2012).
4. M. A. Lampert and P. Mark, *Current Injection in Solids* (Academic, New York, 1970).
5. S. M. Sze, *Physics of Semiconductor Devices*, 2nd ed. (Wiley, New York, 1981).
6. I. Torres, D. M. Taylor, and E. Itoh, Appl. Phys. Lett. **85**, 314 (2004).
7. W. R. Salaneck, K. Seki, A. Kahn, and J.-J. Pireaux, *Conjugated Polymer and Molecular Interfaces* (Marcel Dekker, New York, 2002).

8. B. F. Bory, H. L. Gomes, R. A. J. Janssen, D. M. de Leeuw, and S. C. J. Meskers, J Phys. Chem. C **116**, 12443 (2012).

9. *Electrets*, 3rd ed., edited by G. M. Sessler (Laplacian, California, 1998), Vol. 1.

10. M. Iwamoto, T. Manaka, and D. Taguchi, Jpn. J. Appl. Phys. **53**, 100101 (2014).

11. M. Iwamoto, T. Manaka, T. Yamamoto, and E. Lim, Thin Solid Films **517**, 1312 (2008).

12. M. Iwamoto, T. Manaka, M. Weis, and D. Taguchi, J. Vac. Sci. Technol. B **28**, C5F12 (2010).

13. L. Zhang, D. Taguchi, T. Manaka, and M. Iwamoto, J. Appl. Phys. **110**, 033715 (2011).

14. E. Lim, D. Taguchi, and M. Iwamoto, Appl. Phys. Lett. **105**, 073301 (2014).

15. D. Taguchi, L. Zhang, J. Li, M. Weis, T. Manaka, and M. Iwamoto, J. Phys. Chem. C **114**, 15136 (2010).

16. J. Li, D. Taguchi, W. OuYang, T. Manaka, and M. Iwamoto, Appl. Phys. Lett. **99**, 063302 (2011).

17. D. Taguchi, M. Weis, T. Manaka, and M. Iwamoto, Appl. Phys. Lett. **95**, 263310 (2009).

18. D. Taguchi, S. Inoue, L. Zhang, J. Li, M. Weis, T. Manaka, and M. Iwamoto, J. Phys. Chem. Lett. **1**, 803 (2010).

19. D. Taguchi, L. Zhang, J. Li, M. Weis, T. Manaka, and M. Iwamoto, J. Phys. Chem. C **114**, 15136 (2010).

20. T. Verbiest, K. Clays, and V. Rodriguez, *Second-order Nonlinear Optical Characterization Techniques* (CRC, NY, 2009).

21. R. W. Boyd, *Nonlinear Optics*, 3rd ed. (Academic, MA, 2008).

22. M. Nakamura, N. Sugiyama, Y. Etoh, K. Aosaki, and J. Endo, Nippon Kagaku Kaishi **2001**, 659 (2001).

23. R. Hesse, E. Hoffberger, and H. Bässler, Chem. Phys. **49**, 201 (1980).

24. X. Chen, D. Taguchi, T. Manaka, and M. Iwamoto, J. Appl. Phys. **111**, 113711 (2012).

25. X. Chen, D. Taguchi, T. Manaka, and M. Iwamoto, Appl. Phys. Lett. **104**, 013306 (2014).

26. L. Zhang, D. Taguchi, J. Li, T. Manaka, and M. Iwamoto, Jpn. J. Appl. Phys. **50**, 04DK13 (2011).

27. For example: T. H. Kim, C. K. Song, J. S. Park, and M. C. Suh, IEEE Electron Dev. Lett. **28**, 874 (2007); S. Grecu, A. Opitz, and W. Brütting, Synth. Met. **146**, 359 (2004); T. Sekitani, S. Iba, Y. Kato, Y. Noguchi, T. Someya, and T. Sakurai, Appl. Phys. Lett. **87**, 073505 (2005).

28. For example: C. Goldmann, C. Krellner, K. P. Pernstich, S. Haas, D. J. Gundlach, and

B. Batlogg, J. Appl. Phys. **99**, 034507 (2006); M. Estrada, I. Mejia, A. Cerdeira, and B. Iñiguez, Soli-State Electron. **52**, 53 (2008); J. H. A. Smits, S. C. J. Meskers, R. A. J. Janssen, A. W. Marsman, and D. M. de Leeuw, Adv. Mater. **17**, 1169 (2005).

29. J. Veres, S. D. Ogier, S. W. Leeming, D. C. Cupertino, and S. M. Khaffaf, Adv. Funct. Mater. **13**, 199 (2003).

30. D. Taguchi, T. Shino, L. Zhang, J. Li, M. Weis, T. Manaka, and M. Iwamoto, Appl. Phys. Express **4**, 021602 (2011).

31. J. D. Jackson, *Classical Electrodynamics*, 3rd ed. (Wiley, NY, 1999), Chap. 4.

Figure Captions

Figure 1: (a) Experimental setup for *I-V* measurement coupled with EFISHG measurement of double-layer (Au/pentacene/FP/IZO) diodes. (b) Timing chart of the laser incidence and voltage applied to the diodes for probing the Laplace field $\vec{E}_e + \vec{E}_b$. (c) Timing chart of the laser incidence and voltage applied to the diodes for probing Poisson field $\vec{E}_e + \vec{E}_s + \vec{E}_b$. (d) *I-V* characteristic of the Au/pentacene/FP/IZO diode.

Figure 2: SH spectra of pentacene and FP obtained from Al/pentacene/IZO and Al/FP/IZO single-layer devices.

Figure 3: (a) Results of EFISHG measurements with the square pulse voltage and DC voltage used to probe the Laplace and Poisson fields, respectively. (b) Electric field in the pentacene layer calculated from the EFISHG intensities. (c), (d) Carrier transport mechanism derived on the basis of the EFISHG measurement in the regions (c) $V > 0$ (forward) and (d) $V < 0$ (backward).

Figure 4: *I-E* characteristics of the pentacene and FP layers.

Figure 5: ln(*I*)-$\sqrt{E}$ plot of *I-E* characteristics of the FP layer. The solid and dashed lines show the calculated *I-E* characteristics in the regions $V > 0$ and $V < 0$,

respectively, on the basis of the Schottky-type injection current.

Figure 6: EL spectra of the diode at 0 V, + 20 V (forward), and – 20 V (backward). The inset illustrates the EL measurement setup.

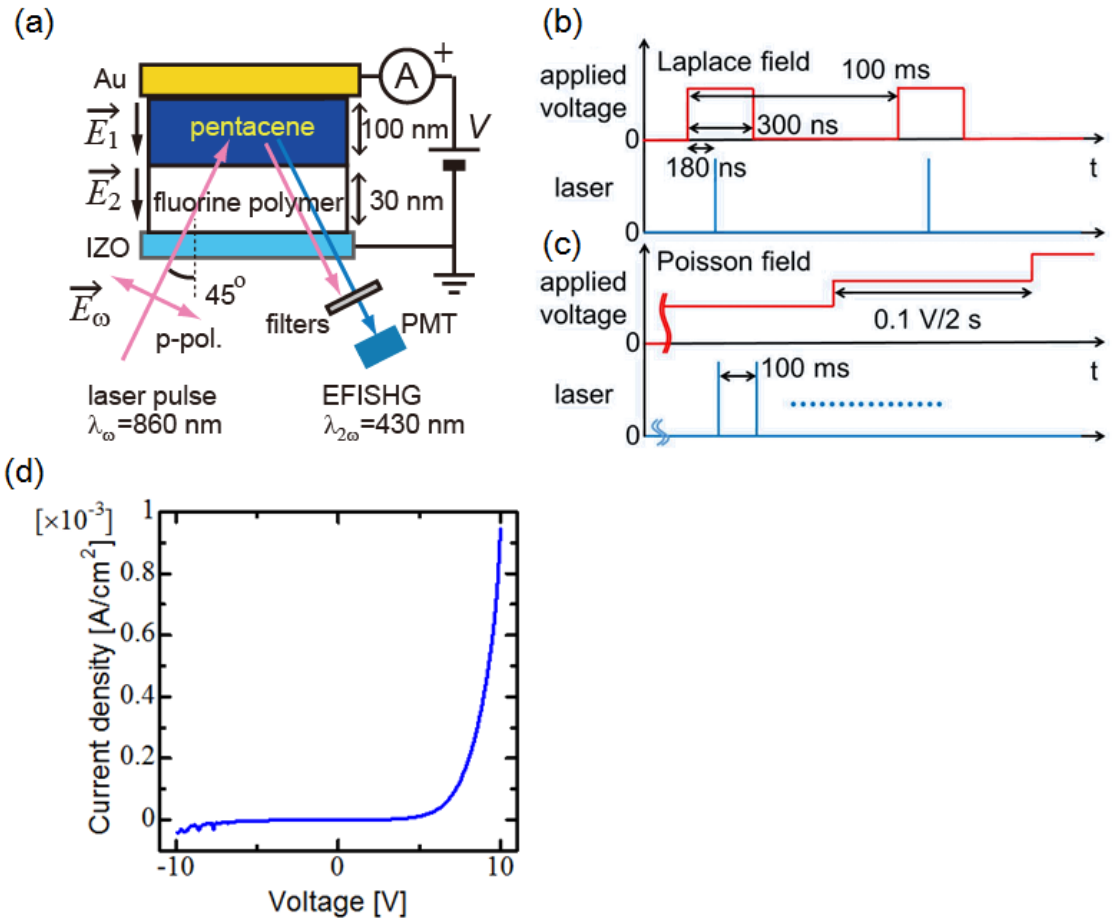

Figure 1: S. Nishi et al.

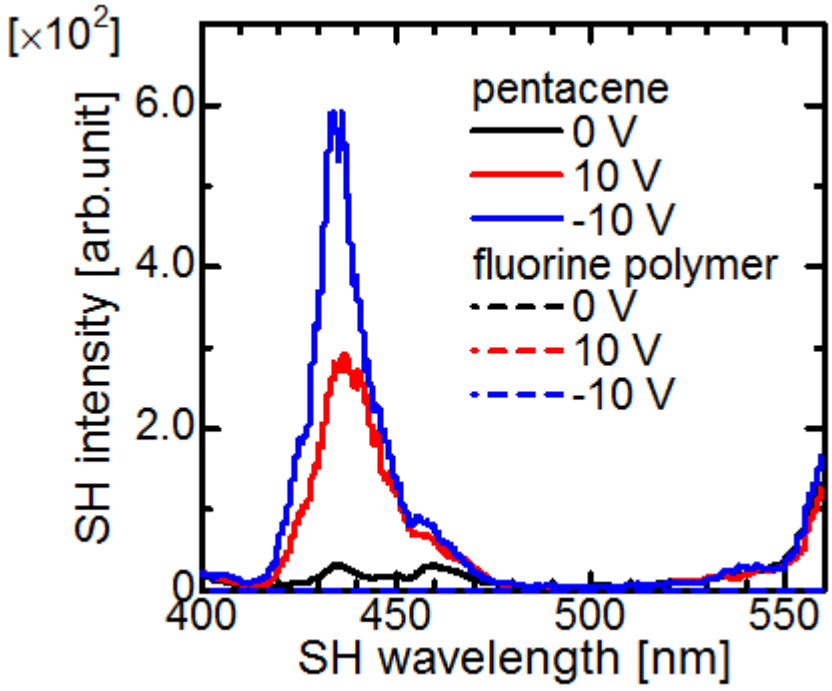

Figure 2: S. Nishi et al.

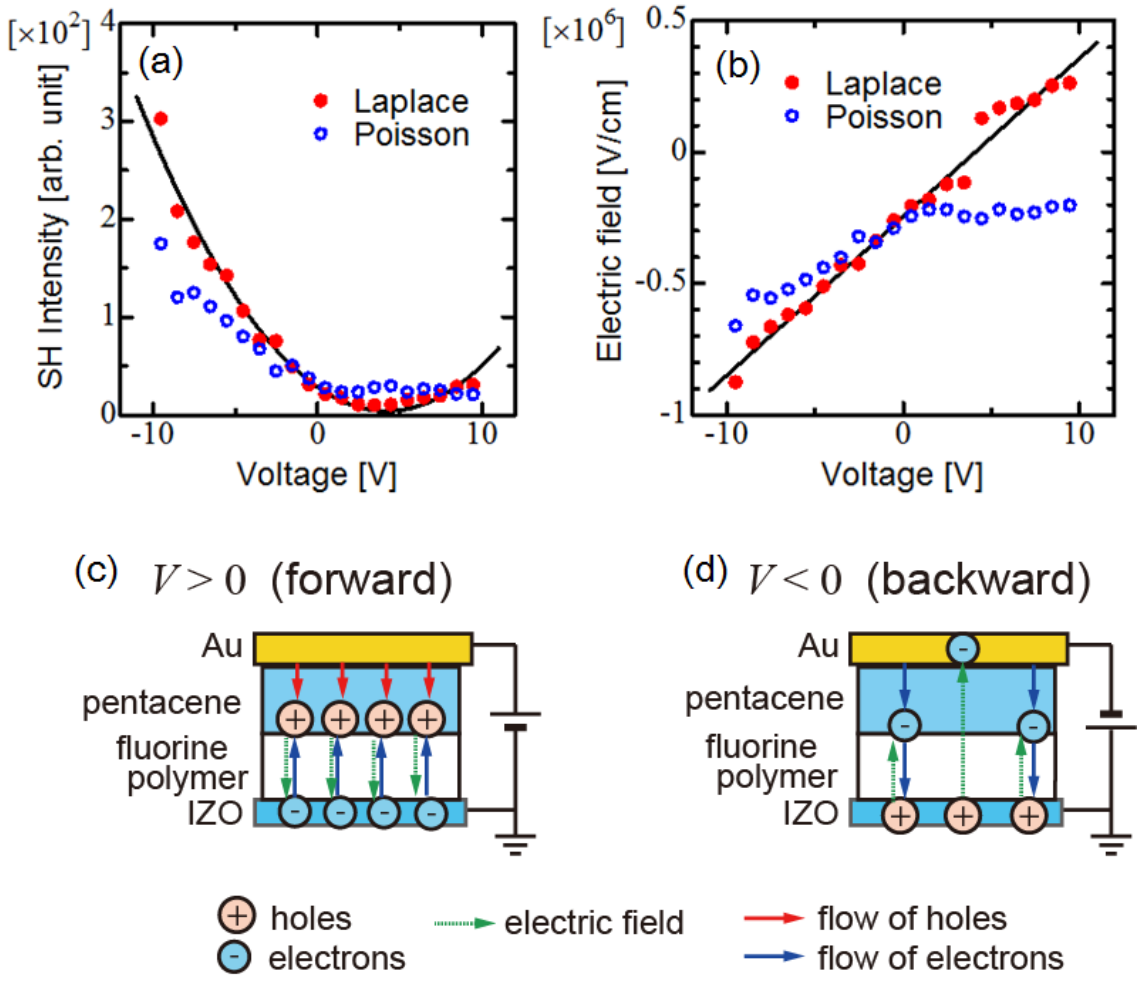

Figure 3: S. Nishi et al.

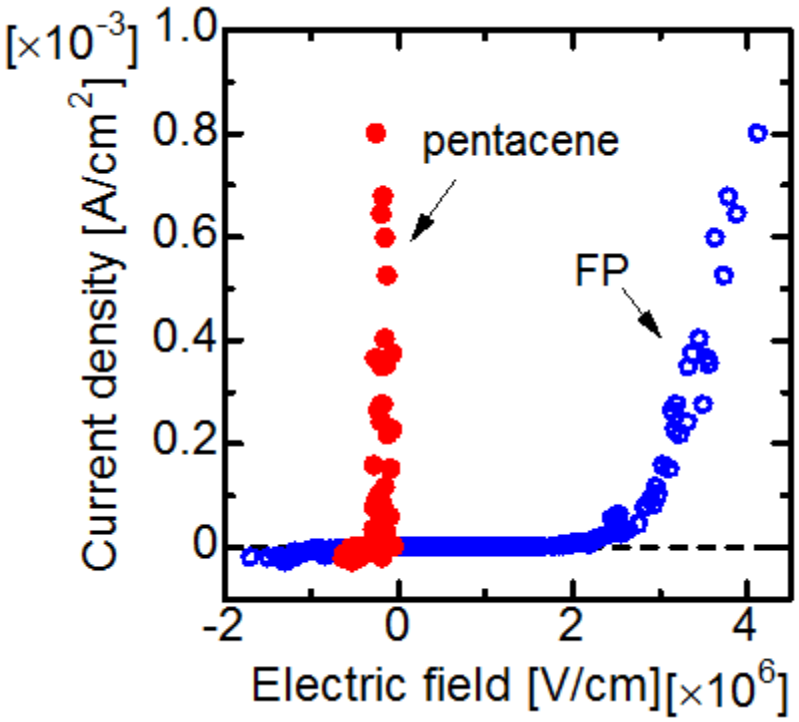

Figure 4: S. Nishi et al.

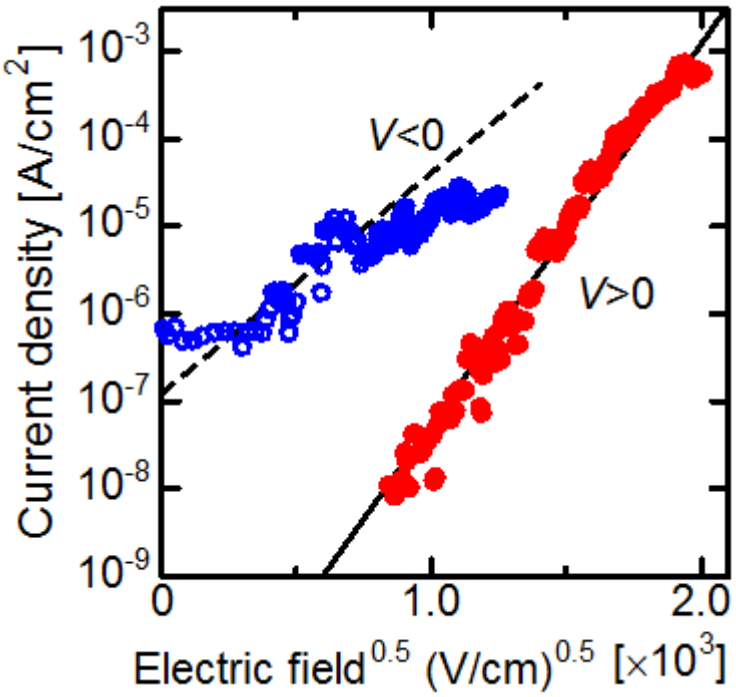

Figure 5: S. Nishi et al.

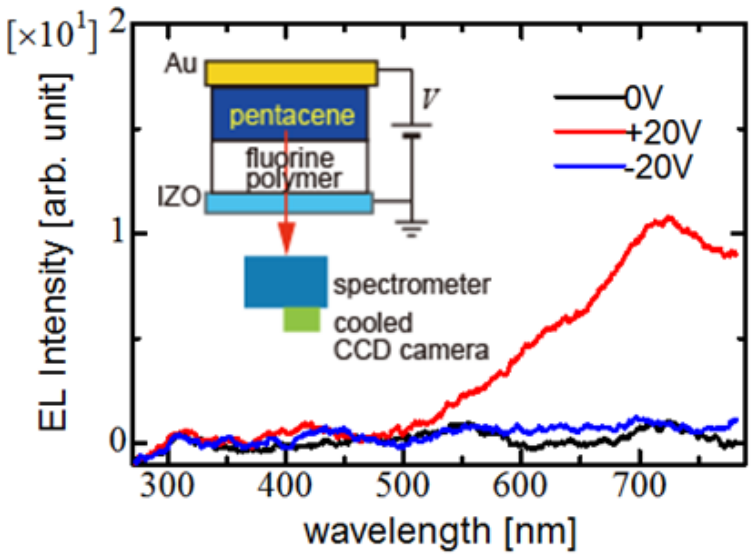

Figure 6: S. Nishi et al.